Variability and Trends in Stratospheric Temperature and Water Vapor

William J. Randel

National Center for Atmospheric Research, Boulder, Colorado, USA

Long-term variability and trends in global stratospheric temperature are described, based on radiosonde observations since the 1960s and satellite measurements since 1979. New radiosonde-based data sets are available that include adjustments for instrumental inhomogeneities, and these data show good agreement with satellite measurements in the lower stratosphere. The stratosphere exhibits well-known transient warming linked to large volcanic eruptions, plus long-term cooling with magnitudes ~−0.5 K/decade in the lower stratosphere to ~−1.2 K/decade in the upper stratosphere. Observations of stratospheric water vapor are also analyzed, based on satellite measurements for 1993–2010. Observed interannual variability is dominated by the quasi-biennial oscillation, plus a step-like drop after 2001. For the observed satellite record, variability in stratospheric water vapor is closely tied to temperature anomalies near the equatorial cold point tropopause.

1. INTRODUCTION

The stratosphere is well-recognized as a key component of the climate system and exhibits coupling to the troposphere across synoptic to decadal time scales. Temperature changes and trends in the stratosphere are an important aspect of global change and are crucial for interpreting and understanding anthropogenic climate change and stratospheric ozone trends (including predictions of future changes). The observed variability and trends in temperatures provides a fingerprint of key processes that influence the stratosphere and are fundamental diagnostics for evaluating model simulations [e.g. *Garcia et al.*, 2007; *Intergovernmental Panel on Climate Change*, 2007; *Austin et al.*, 2009; *SPARC*, 2010].

The historical observational record of global stratospheric temperature is relatively short compared to surface climate records, beginning in the late 1950s for the lower stratosphere (from balloon measurements) and in 1979 for the middle and upper stratosphere (based on satellite data). Furthermore, these historical data were intended for use in operational weather analysis and forecasting and not for producing high-quality climate records, and the measurement record is plagued by artificial effects linked to changes in instrumentation or observational practices (such as improvements in radiosonde instruments or changes in operational satellites) [e.g., *Gaffen*, 1994; *Lanzante et al.*, 2003a]. Such artificial effects are important to take into account when trying to quantify relatively small climate signals. This problem is now well-recognized, and several research groups have developed techniques to make adjustments in historical data and produce climate data sets (for both radiosondes and satellites). Because the artificial changes can be subtle and difficult to identify in the presence of natural variability, it is valuable to have independent analyses of the data sets (and these then provide one measure of uncertainty in the final products). One objective of this paper is to give an overview of stratospheric temperature variability and trends from the historical record and briefly discuss current understanding of this variability. Six separate stratospheric temperature data sets have recently been reviewed by *Randel et al.* [2009a], and the results here focus on overall behavior from a few of those data sets.

Stratospheric water vapor is important because of its radiative effects on stratospheric temperature and surface climate [e.g., *Forster and Shine*, 1999; *Solomon et al.*, 2010],

The Stratosphere: Dynamics, Transport, and Chemistry
Geophysical Monograph Series 190

10.1029/2009GM000870

and chemical effects on ozone [*Dvortsov and Solomon*, 2001]. Air enters the stratosphere primarily in the tropics and is dehydrated on passing the cold tropical tropopause, and this accounts for the overall extreme dryness of the stratosphere [*Brewer*, 1949]. The annual cycle of tropical tropopause temperatures (8 K maximum to minimum) furthermore imparts a strong seasonal cycle (approximately 3.0 to 4.5 ppmv) to stratospheric water vapor near the tropopause, which then propagates coherently throughout the stratosphere [*Mote et al.*, 1996]. *Fueglistaler et al.* [2005] showed that the observed seasonal cycle can be accurately simulated using Lagrangian trajectory calculations (based on analyzed large-scale temperature and wind fields), confirming freeze-out near the cold point as a simple explanation of the large seasonal variation. Interest in stratospheric water vapor increased substantially following the observations of large positive trends (~10% per decade) from a long record of balloon measurements by *Oltmans and Hoffman* [1995]. More recently, satellites have provided global observations and increasingly long records of stratospheric water vapor, and substantial effort has focused on quantifying and understanding interannual variability in both satellite and balloon data [e.g., *Stratospheric Processes and Their Role in Climate* (*SPARC*), 2000; *Randel et al.*, 2004; *Fueglistaler and Haynes*, 2005; *Scherer et al.*, 2008]. Analyses of seasonal and interannual changes in water vapor are now a standard diagnostic for stratospheric model simulations [e.g., *Eyring et al.*, 2006; *Garcia et al.*, 2007; *Oman et al.*, 2008; *SPARC*, 2010]. Here an update of the satellite-based record covering 1993–2010 is presented, including comparisons with tropical tropopause temperatures over this period, and inferences regarding the control of interannual changes in stratospheric water vapor are discussed.

2. TEMPERATURE DATA

Historical observations of stratospheric temperature are primarily derived from radiosonde (balloon) and satellite measurements. Radiosonde measurements in the lower stratosphere extend back to the late 1950s, although regular global coverage above 100 hPa did not occur until after approximately 1965. A key aspect of the radiosonde record is that there have been changes in instrumentation and observational practice over the 50-year period, so that the raw radiosonde record contains substantial inhomogeneities that particularly influence the stratosphere [e.g., *Gaffen*, 1994; *Lanzante et al.*, 2003a]. One important problem is that the older measurements often have systematic warm biases in the stratosphere (related to radiation effects on the temperature sensor), so that time series can include artificial cooling biases. These trend biases can be as large as or larger than the true climate signal [*Lanzante et al.*, 2003b], and these artificial effects require correction before reliable stratospheric trends can be estimated. This problem is well recognized in the research community, and several radiosonde-based data sets have been developed during the last several years, which employ a variety of techniques to isolate and correct data inhomogeneities. *Randel et al.* [2009a] discuss and compare results from six such data sets, and the overall variability is similar among these data (although trend estimates can vary substantially in some regions). Here we focus on results from two of these data sets, which show good overall agreement with satellite measurements. The Radiosonde Atmospheric Temperature Products for Assessing Climate (RATPAC) [*Free et al.*, 2005] is a data set based on an 85-station network, whose data are adjusted using the approach described by *Lanzante et al.* [2003a, 2003b]. The so-called RATPAC-lite data set is a 47-station subset of the RATPAC data, where satellite-radiosonde comparisons have been used to isolate and remove stations with remaining inhomogeneities [*Randel and Wu*, 2006; *Randel et al.*, 2009a]. The RATPAC-lite data cover the period beginning in 1979. We also use the Radiosonde Innovation Composite Homogenization (RICH) data set [*Haimberger et al.*, 2008], which uses meteorological reanalyses to identify artificial break points in radiosonde time series, which are then adjusted using neighboring radiosonde comparisons. While the RICH data extend back to 1958, we note that there are substantial uncertainties in all the radiosonde data sets for the presatellite era, especially for the data sparse tropics and Southern Hemisphere (SH) [*Randel et al.*, 2009a].

Near-global satellite observations of stratospheric temperatures started in the early 1970s, with the first continuous series of observations beginning in the late 1970s with the NOAA operational satellites. These instruments include the Microwave Sounding Unit (MSU) and the Stratospheric Sounding Unit (SSU), which provide ~10–15 km thick layer-mean temperatures for a number of layers spanning the lower to upper stratosphere [see *Randel et al.*, 2009a]. A key point is that individual satellite instruments are relatively short-lived, so that data from 13 different satellites have been used since 1979. This presents challenges for creating climate quality data sets, as each instrument has slightly different calibration characteristics, the orbits differ between satellites and drift for individual satellites (which can alias stratospheric diurnal tides into trends), and the overlap period between different satellites is sometimes small. For the MSU Channel 4 (hereafter MSU4) data (covering ~13–22 km), there are two separate analyses that are routinely updated for the long-term record, from Remote Sensing Systems [*Mears and Wentz*, 2009] and from the University of Alabama at Huntsville

(UAH) [*Christy et al.*, 2003]. There are relatively small differences between these MSU4 data sets, and we focus here on the UAH analyses; note the last MSU instrument ceased operation in 2005, and the time series have been extended to present using data from a very similar channel on the Advanced Microwave Sounding Unit since 1998. SSU measurements are available from 1979 to 2005 and are the only near-global source of temperature measurements above the lower stratosphere over this period. The SSU data include measurements for three nadir-viewing channels, plus several synthetic so-called x-channels, which combine nadir and off-nadir measurements [*Nash and Forrester*, 1986]. The time series shown here combine measurements for seven separate SSU instruments and are an extension of the time series derived by *Nash and Forrester* [1986] and *Nash* [1988]; one key uncertainty is that this is the only analysis of the combined SSU data to date. The SSU data have been corrected to account for effects of increasing atmospheric CO_2 on the measurements, which result in systematically raising the altitude of the SSU weighting functions and positively biasing resulting temperature trends [*Shine et al.*, 2008].

3. TEMPERATURE OBSERVATIONS

An overview of lower stratospheric temperature variability for the period 1960–2008 is shown in Figure 1, which shows

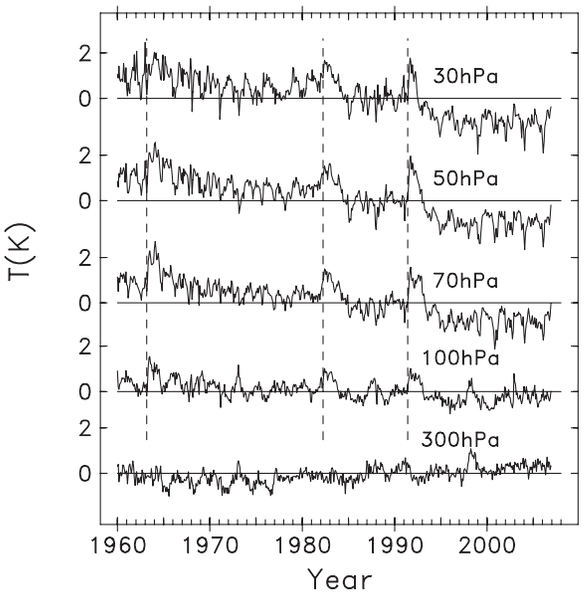

Figure 1. Time series of global average temperature anomalies at pressure levels spanning the upper troposphere to lower stratosphere, derived from the RICH data. The dashed lines denote the volcanic eruptions of Agung (March 1963), El Chichon (April 1982), and Mount Pinatubo (June 1991).

deseasonalized global-mean temperature anomalies at individual pressure levels 300–30 hPa, based on the RICH data. In the stratosphere, the primary components of global variability are the transient warming events linked to the volcanic eruptions of Agung (March 1963), El Chichon (April 1982), and Mount Pinatubo (July 1991), together with long-term net cooling changes of ~2 K. The 300-hPa time series in Figure 1 is included to contrast upper tropospheric temperature behavior, which shows long-term warming, and episodic variations tied to the El Niño–Southern Oscillation (ENSO). The spatial structure of the linear trend and ENSO variations in the zonal mean RICH temperature data for the period 1970–2006 are shown in Figure 2, derived from a standard multivariate linear regression analysis (described in Appendix A). The linear trends in Figure 2a show warming in the troposphere (largest in the NH extratropics and in the tropical upper troposphere) and cooling in the stratosphere. Although the time series in Figure 1 shows that the long-term stratospheric changes are not linear (possibly more step-like) [e.g., *Seidel and Lanzante*, 2004], the linear trends provide a concise measure of net long-term changes. There are substantial latitudinal gradients in trends over 10–15 km linked to the sloping tropopause in Figure 2a, which will lead via the thermal wind relation to increased subtropical jets above 10 km. In the stratosphere above 100 hPa, the trends in Figure 2a show a relatively flat latitudinal structure outside of polar regions. The RICH trends show somewhat larger cooling near the equator and over the SH at 30 and 50 hPa in Figure 2a, but this detail may be suspect because of data uncertainties in these regions.

Zonal mean temperature variations associated with ENSO (Figure 2b) show coherent variations throughout the tropical troposphere, which are approximately in-phase (a 1-month lag) with the multivariate ENSO index, which we use to statistically model ENSO variability (see Appendix A). Note that while Figure 2b shows the zonal mean signature, there is also strong longitudinal (planetary wave) structure to the ENSO temperature response [e.g., *Yulaeva and Wallace*, 1994; *Calvo Fernandez et al.*, 2004]. The ENSO pattern in Figure 2b shows an out-of-phase response in the tropical lower stratosphere (near 70 hPa) that is of similar magnitude to the tropospheric signal and is associated with local temperature variations of ±1 K. A time series of stratospheric temperatures in this region is shown in Figure 3, together with the components associated with separate terms in the regression fit. The ENSO and quasi-biennial oscillation (QBO) components are of similar amplitude at this location, and the net response often depends on the relative phasing of the two signals (for example, there is a near cancellation of these signals during the large ENSO event of 1997–1998, whereas an in-phase behavior in 2000 results in a relatively large net

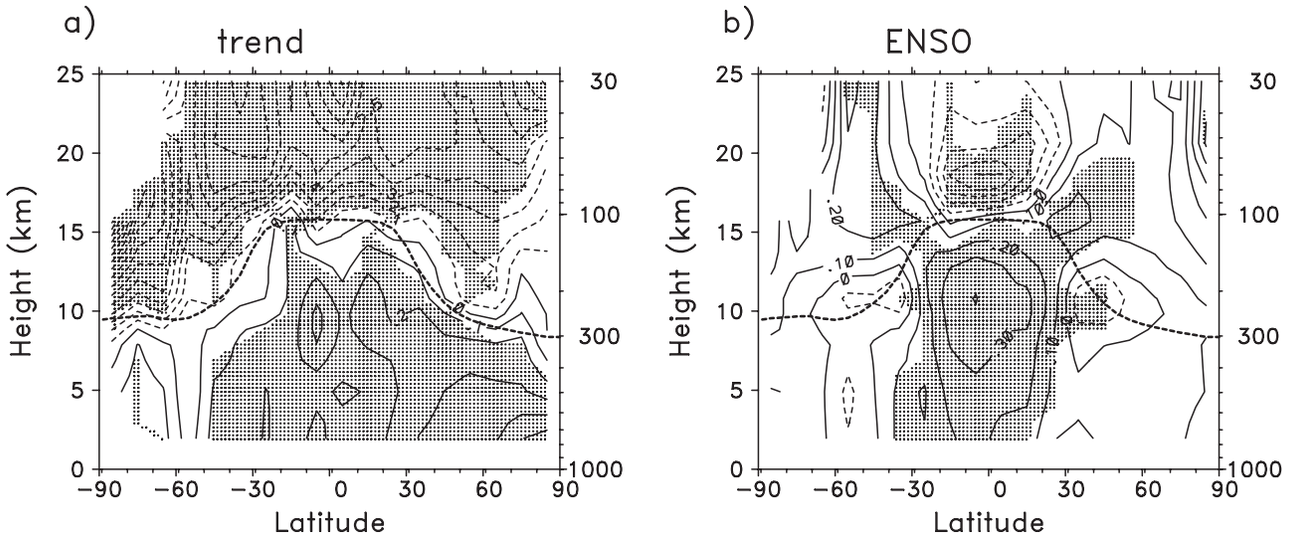

Figure 2. Cross sections of (a) linear trends (contour interval of 0.1 K/decade) and (b) El Niño–Southern Oscillation (ENSO) temperature variations (contour interval of 0.1 K/multivariate ENSO index) in zonally averaged RICH data, for the period 1970–2006. In both plots, solid and dashed lines denote positive and negative values, and shaded regions denote the statistical fits are significant at the 2-sigma level. The dark dashed line denotes the tropopause.

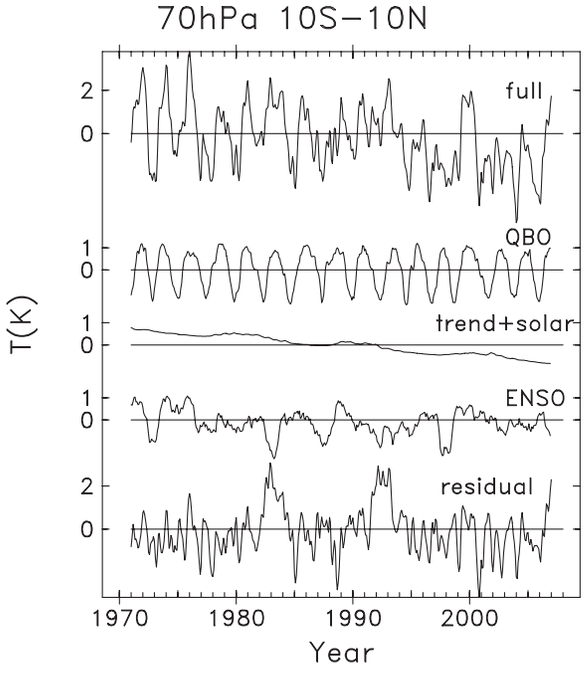

Figure 3. Top curve shows time series of zonal mean temperature at 70 hPa over 10°N–10°S from the RICH data during 1970–2006. The lower curve shows components of variability derived from the multivariate regression fit, together with the residual (bottom curve). Note that the volcanic warming signals of El Chichon (1982) and Pinatubo (1991) are clearly seen in the residual time series, although they are not evident amid the other variability in the full time series.

anomaly). The importance of both the ENSO and QBO variations in this region was previously discussed by *Reid* [1994]. *Free and Seidel* [2009] furthermore show a large ENSO signal in the Arctic stratosphere that maximizes during winter (not evident in the annual mean results shown in Figure 2b).

Figure 4 shows the spatial structure of the temperature anomalies associated with the El Chichon and Pinatubo volcanic eruptions. These are calculated based on the residuals to the full regression fit (see Appendix A and Figure 3), taking the difference between the temperature for 1 year following each eruption and the previous 3 years. Both eruptions result in warm temperatures of 2–3 K centered in the tropical stratosphere (somewhat larger and situated higher for Pinatubo). These temperature anomalies persist for 1–2 years after each eruption (Figure 1). The volcanic periods are also linked to significant cooling in the troposphere, and these volcanic signals provide sensitive tests of tropospheric climate feedback process [*Soden et al.*, 2002]. These volcanic temperature variations have been discussed in more detail by *Free and Angell* [2002], who also analyze the patterns associated with Agung (which shows more asymmetry, with stratospheric warming shifted toward the SH).

Figure 5 shows time series of deseasonalized global-average MSU4 satellite temperature anomalies, together with equivalent results from the RICH and RATPAC-lite radiosonde data (integrated with the MSU4 weighting functions). This compares the direct global satellite measurements with

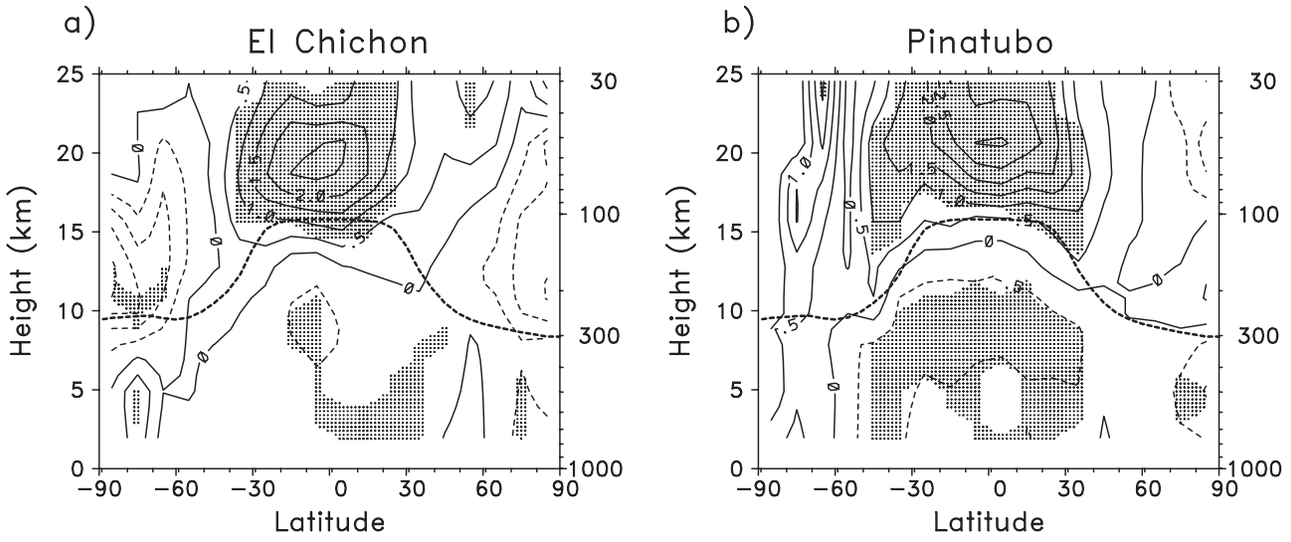

Figure 4. Cross sections of temperature anomalies associated with the (a) El Chichon and (b) Mount Pinatubo volcanic eruptions. These anomalies are estimated from the residuals to the multivariate regression fit (see Appendix A), taking the difference between the 1-year average after each eruption and the previous 3 years. Shading denotes regions where the anomalies are greater than twice the standard deviation of annual mean temperature anomalies at each location. The dark dashed line indicates the tropopause.

equivalent radiosonde-based data sets. The overall behavior of MSU4 is very similar to the 70- to 50-hPa time series in Figure 1, with volcanic effects and step-like temperature decreases (and relatively constant temperatures since ~1995). There is excellent agreement in detail between the satellite measurements and the integrated (homogeneity-adjusted) radiosonde data, and this agreement is a substantial improvement over similar comparisons using unhomogenized data [*Randel and Wu*, 2006]. The longer record from RICH data provides a longer perspective on the recent record, including the clear signature of the Agung volcanic eruption in 1963.

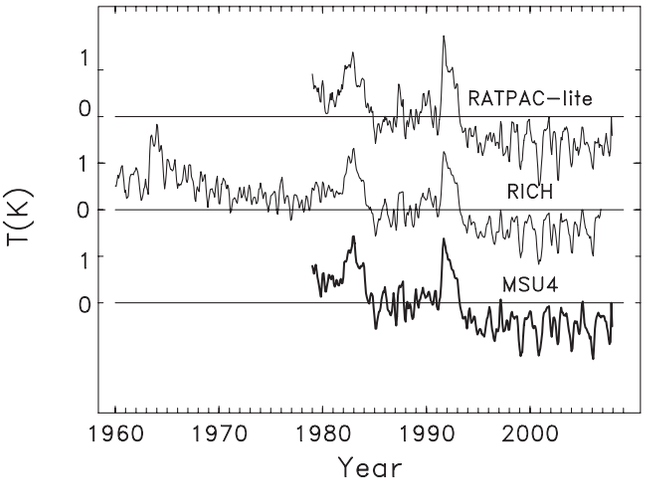

Figure 5. Time series of global mean temperature anomalies from MSU4 satellite data, together with corresponding time series derived from the RICH and RATPAC-lite data sets (vertically integrated using the MSU4 weighting function). Each time series has been normalized to zero for the period 1985–1990.

The vertical profile of linear trends over 1979–2006 in the RICH and RATPAC-lite data are shown in Plate 1, for tropical and extratropical latitude bands, together with corresponding trends derived from the UAH MSU4 data. Trends calculated from the two radiosonde data sets agree well, with the RICH data showing somewhat larger cooling at uppermost levels and slightly different vertical structure in the tropics (including the altitude of the crossover from tropospheric warming to stratospheric cooling). The MSU4 satellite trends show reasonable agreement with the radiosonde results, and overall, the trends show a relatively flat (approximately constant) latitudinal structure over 60°N-S.

Stratospheric temperature changes at polar latitudes deserve separate attention because of the high level of (natural) year-to-year variability during winter and spring. This well-known behavior [e.g., *Labitzke and van Loon*, 1999; *Yoden et al.*, 2002] is illustrated in Figure 6, which shows 70 hPa polar temperature anomalies for seasonal averages (December-January-February (DJF), March-April-May (MAM), etc.) for both the Arctic (60°N–90°N) and Antarctic (60°S–90°S). Large year-to-year variability is observed in the Antarctic during spring (September-October-November (SON)) and in the Arctic during winter (DJF). Long-term

cooling trends are evident in the SH during spring (SON) and summer (DJF), and these are associated with development of the Antarctic ozone hole after 1980 [*Randel and Wu*, 1999]. Plate 2b shows the vertical profile of seasonal temperature trends in the Antarctic (for 1970–2006), highlighting cooling throughout the lower stratosphere during spring and summer. Arctic time series (Figure 6a) and trends (Plate 2a) show cooling during summer (June-July-August (JJA)), which is statistically significant because of low natural variability during this season.

Temperature observations in the middle and upper stratosphere derived from the SSU data are available from 1979 to 2005, and Figure 7 shows time series of near-global (60°N–60°S) anomalies for several SSU channels (along with MSU4 for comparison). Time series show overall cooling throughout the stratosphere, with largest net changes (~3 K) in the upper stratosphere. The changes are not monotonic, however, with the transient warming of the El Chichon and Pinatubo eruptions evident from the lower through the middle stratosphere (in SSU channel 26). The upper stratosphere (SSU channels 27 and 36x) shows the influence of long-term cooling superimposed on the 11-year solar cycle (with maxima centered near 1980, 1991, and 2002), which results in a stair-step structure. As with the lower stratosphere, temperatures were relatively constant in the middle and upper stratosphere during 1995–2005.

The vertical structure of near-global mean temperature trends throughout the stratosphere during 1979–2005 is shown in Plate 3, combining results for the SSU and MSU satellites, plus radiosonde data. The overall pattern shows trends increasing with altitude from the lower (~−0.5 K/decade) to upper stratosphere (~−1.2 K/decade). There is good agreement between the radiosonde and satellite-derived trends for the region where they overlap. Unfortunately, there are no independent measurements of upper stratospheric temperatures on a global scale to compare with the SSU trend results. Long-term measurements of temperatures over 30–80 km from lidar measurements are available from a few stations [*Keckhut et al.*, 2004]. *Randel et al.* [2009a] show there is reasonable overall agreement between the SSU satellite data and lidar measurements from three stations with the longest records (i.e., the statistical trend uncertainties overlap), although there are large differences in sampling that preclude constraining trend uncertainties in either the satellite or lidar data sets.

4. STRATOSPHERIC WATER VAPOR

Observations of stratospheric water vapor have been made by balloon, aircraft, and satellite measurements (as reviewed by *SPARC* [2000]). Estimates of long-term variability and trends derived from combining different data sets are

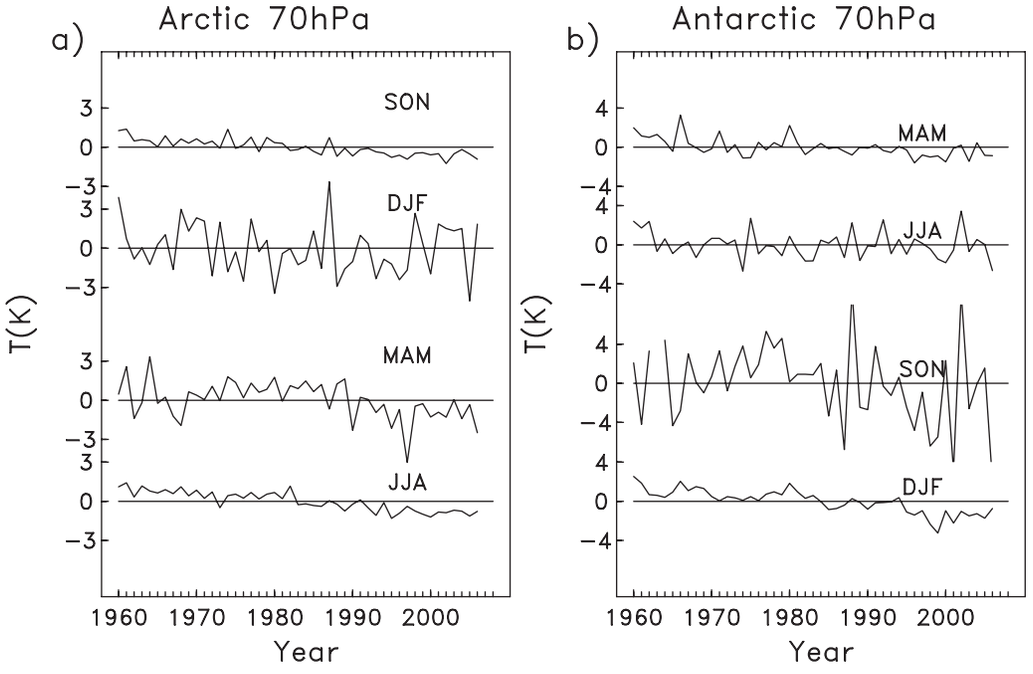

Figure 6. Time series of 70 hPa temperature anomalies in the (a) Arctic (60°N–90°N) and (b) Antarctic (60°S–90°S), calculated from RICH data for each season (December–January–February, DJF, etc.).

problematic because of the relatively large uncertainties and biases (~10%–20%) among different data and measurement techniques [*SPARC*, 2000]. The longest time series of observations from a single location are from balloon measurements from Boulder, Colorado, which began in the early 1980s, with the sampling of individual profiles approximately once per month (or less). These data have been examined in a number of analyses [*Oltmans and Hoffman*, 1995; *Oltmans et al.*, 2000; *Scherer et al.*, 2008; *Solomon et al.*, 2010] and show an overall increase of water vapor since 1980 but with significant variability associated with individual (snapshot) profile measurements.

Global satellite observations allow vastly improved space-time sampling of stratospheric water vapor, so that large-scale coherent variability can be examined in detail, but these are limited in terms of long-term measurements. Here we examine satellite data from the Halogen Occultation Experiment (HALOE) covering January 1992 to August 2005 (using retrieval version v19), combined with Aura Microwave Limb Sounder (MLS) for the period June 2004 to May 2010 (v2.2), and produce a single time series by adjusting the data using the overlap period during 2004–2005. HALOE is based on solar occultation measurements [*Russell et al.*, 1993], which have high vertical resolution (~2 km) but limited spatial sampling (requiring approximately 1 month to sample the region 60°N–60°S). The MLS data [*Read et al.*, 2007] have somewhat lower vertical resolution (~ 3 km), but much denser spatial sampling, with near-global coverage everyday.

While both HALOE and MLS provide high-quality measurements, there are systematic differences of order 10% between the data (related to vertical resolution and retrieval details) that require adjustment to produce a single continuous data set. Here we simply deseasonalize both the HALOE and MLS data sets individually (which removes the systematic bias) and then adjust the MLS anomalies to match the HALOE data for the overlap period June 2004 to August 2005. The results are illustrated in Plate 4a, which shows near-global (50°N–50°S) anomalies for the HALOE and MLS data at 82 hPa over 1993–2008. The overlap period is highlighted in Plate 4b, showing reasonable agreement between interannual anomalies derived from both data sets (the

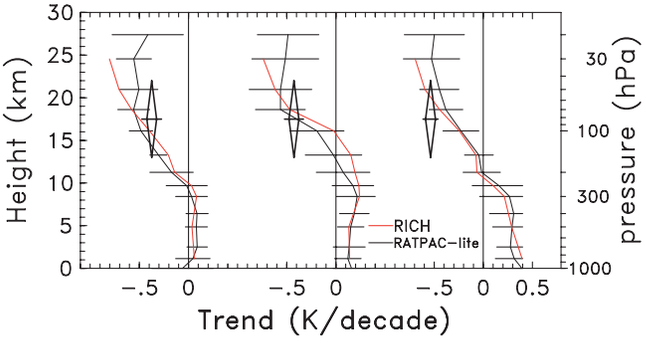

Plate 1. Vertical profile of temperature trends during 1979–2007 derived from RICH and RATPAC-lite data, for latitude bands 30°S–60°S, 30°N–30° S, and 30°N–60°N (left to right). The diamonds denote corresponding trends derived from the UAH MSU4 data, and the height of the diamond corresponds to the MSU4 weighting function. Error bars denote the 2-sigma statistical trend uncertainties.

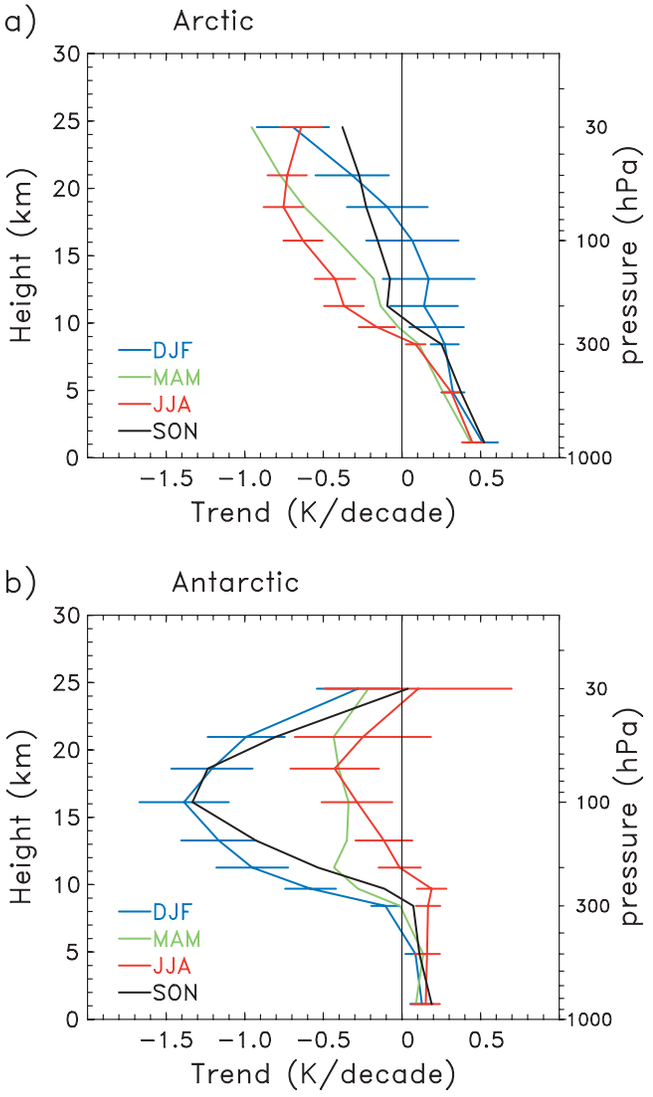

Plate 2. Vertical profile of temperature trends for 1979–2006 over the (a) Arctic (60°N–90°N) and (b) Antarctic (60°S–90°S), based on RICH radiosonde data. Trends are calculated for each season, and error bars denote 1-sigma uncertainties (for clarity, shown only for DJF and JJA statistics).

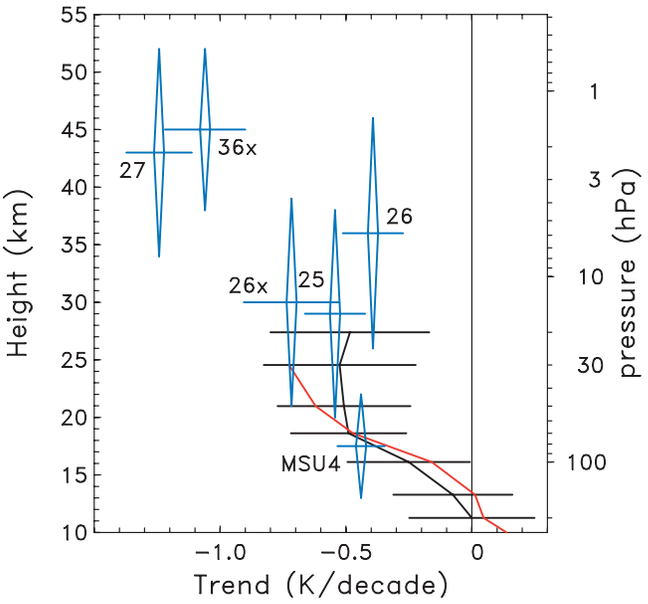

Plate 3. Vertical profile of near-global (60°N-S) temperature trends over 1979–2005 derived from satellite and radiosonde data sets. The lines in the lower stratosphere indicate trends from the RICH (red) and RATPAC-lite (black) data. Blue diamonds indicate trends from MSU4 and SSU satellite data, with the height of the diamond representing the respective weighting function. Error bars denote 2-sigma statistical trend uncertainties.

anomalies for this period are primarily related to the QBO). Note the month-to-month variability in Plate 3 is somewhat smoother in the MLS data, probably due to the denser space-time sampling compared to HALOE. This approximate agreement in variability during the overlap period provides confidence for using the MLS data to extend the HALOE record.

The overall behavior of water vapor interannual changes in the lower stratosphere (Plate 4a) show variations with an approximate 2-year periodicity, related to the QBO influence on tropical tropopause temperature, combined with a significant drop in water vapor (~0.4 ppmv) after ~2001 and a suggestion of recent increasing values. These interannual variations in water vapor originate near the tropical tropopause and propagate to higher latitudes of both hemisphere in the lower stratosphere and also to higher altitudes in the tropics [*Randel et al.*, 2004]. Plate 5 shows a height-time section of near-global (50°N-S) average water vapor anomalies from 1993–2010, showing this vertical propagation and highlighting the tropopause as a source region for the global anomalies.

Brewer [1949] proposed a simple mechanism by which tropical tropopause temperatures control stratospheric water vapor, and observations [*Randel et al.*, 2004] and trajectory calculations [*Fueglistaler et al.*, 2005; *Fueglistaler and Haynes*, 2005] have confirmed this for both the annual cycle and interannual changes. This behavior is demonstrated for the time series over 1993–2010 in Plate 6, which shows the 82-hPa global water vapor fluctuations together with anomalies in tropical tropopause (cold point) temperatures. This latter time series is derived from a small group of near-equatorial radiosonde stations, chosen based on wide spatial sampling and consideration of data quality (via comparison with MSU satellite data, as described in the work of *Randel and Wu* [2006]). These stations include Nairobi (1°S, 37°E), Majuro (7°N, 171°E), and Manaus (3°S, 60°W), and the time series for each station is shown in Figure 8, showing overall

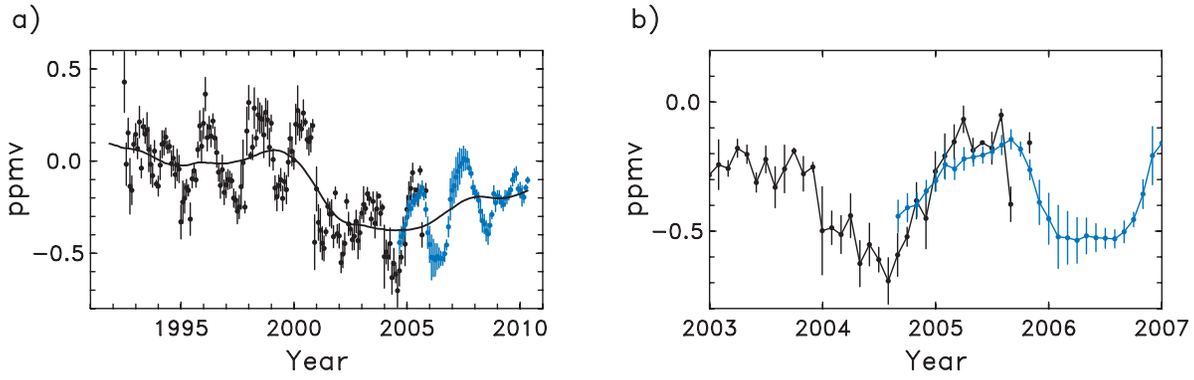

Plate 4. (a) Time series of deseasonalized near-global (50°N–50°S) water vapor anomalies in the lower stratosphere (82 hPa) during 1993–2008. Black points show data derived from the Halogen Occultation Experiment (HALOE) measurements, and blue points from Aura Microwave Limb Sounder (MLS). The black line is a smooth fit to the data, using a Gaussian smoother with a half-width of 1 year. (b) A highlight of the overlap period during 2004–2005, illustrating how the MLS anomalies are adjusted to match the HALOE data to construct a continuous record. The vertical bars denote the standard deviation of the near-global anomalies for each month.

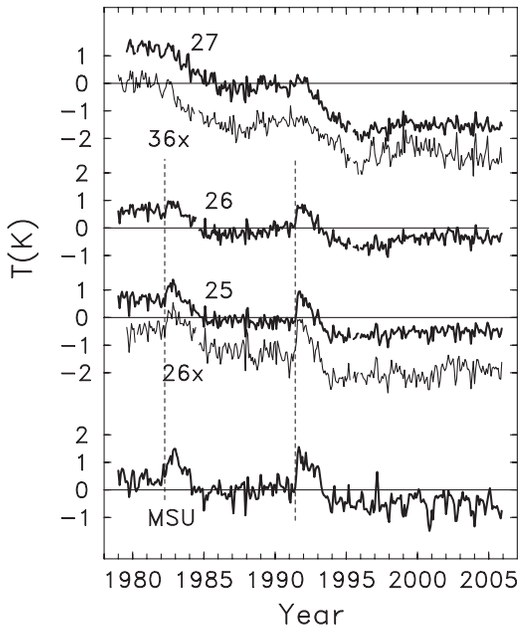

Figure 7. Time series of near-global (60°N–60°S) temperature anomalies from satellite data covering the lower to upper stratosphere, for the period 1979–2005. The lower curve shows results for MSU4, and the upper curves show results for separate SSU channels spanning the middle to upper stratosphere (with approximate altitudes indicated in Plate 3). The SSU data series ends in 2005. The dashed lines indicate the El Chichon and Pinatubo volcanic eruptions.

coherent behavior for anomalies in cold point temperature among the stations. Note that the cold point tropopause is typically near 90–105 hPa, not at a standard pressure level, and thus, cold point anomalies are not available in the homogenized (standard pressure level) radiosonde data sets such as RICH or RATPAC. There is a high level of agreement between the tropopause temperature and water vapor anomalies in Plate 6, with a correlation of 0.76 (with water vapor lagging temperature by 2 months). Both the QBO variations and the decrease after 2001 are observed in both time series. The relationship in Plate 6 suggests a water vapor-temperature sensitivity of ~0.5 ppmv K^{-1}, and this value is consistent with results derived from the trajectory calculations of *Fueglistaler and Haynes* [2005], which are based on large-scale meteorological analyses and assumption of 100% saturation of water vapor with respect to ice. This observed correlation suggests a relatively simple control of global stratospheric water vapor by freeze drying near the tropical tropopause, at least for the period 1993–2010, when global-scale measurements of water vapor from satellites are available.

The main component of interannual variability for water vapor in Plate 6 is due to the QBO, and that is why the near-equatorial radiosonde measurements (stations within ±10° of the equator) show strongest correlations. Figure 8 also shows time series of temperature anomalies at 100 and 70 hPa (slightly below and above the cold point). While there is coherence among the temperature variations over these nearby levels, the strongest correlation to stratospheric water vapor anomalies is found for the cold point. Also, the relatively abrupt decrease in temperature after 2001 (echoed in stratospheric water vapor) is most evident at the cold point, and this behavior reinforces the relatively simple picture of water vapor control by freeze-out near the equatorial cold point. *Rosenlof and Reid* [2008] also discussed correlations of stratospheric water vapor with temperatures near the tropical tropopause, noting the strong changes after 2001, although *Lanzante* [2009] pointed out large potential biases in the associated radiosonde data, due to unadjusted instrumental changes.

5. SUMMARY AND DISCUSSION

Interannual variability in stratospheric temperature is linked to forcing associated with large volcanic events, long-term changes (trends) in radiative gases, and solar variability, in addition to dynamical variability linked to the QBO and ENSO, and natural year-to-year variations (which are largest in the winter-spring polar regions). Each of these forced

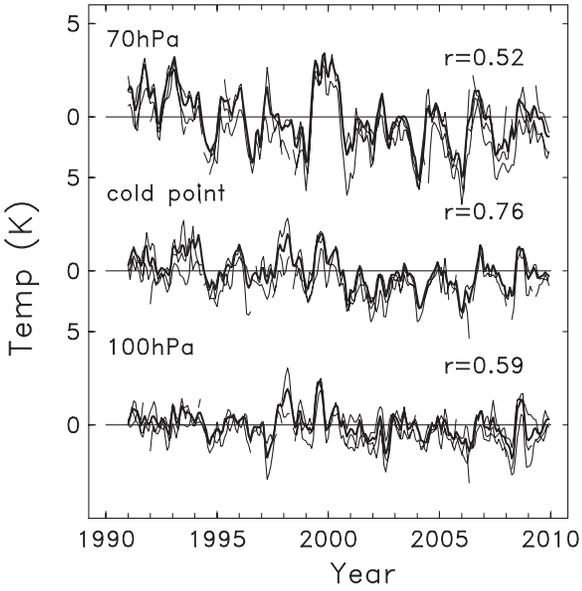

Figure 8. Time series of deseasonalized temperature anomalies derived from several near-equatorial radiosonde stations at 100 hPa, the cold-point tropopause, and 70 hPa. The thin lines show results at each of three stations (Nairobi, Majuro, and Manaus), and the thick line is the average. Correlations with lower stratospheric water vapor (time series in Plate 6 are indicated for each level).

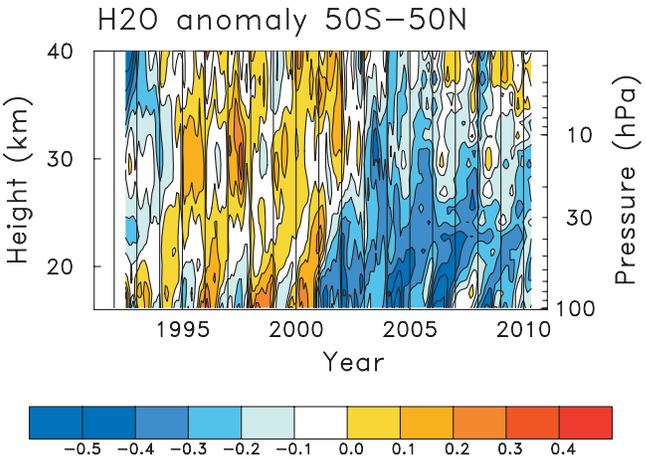

Plate 5. Height-time section of near-global (50°N–50°S) deseasonalized water vapor anomalies (as in Plate 4a) throughout the stratosphere over 1993–2008.

signals is relatively well understood and simulated to some degree in current stratospheric chemistry-climate models [*SPARC*, 2010]. In the global mean, the changes do not appear monotonic, but rather step-like; this behavior has been examined and discussed by *Seidel and Lanzante* [2004] and *Ramaswamy et al.* [2006]. The long-term cooling of the stratosphere is linked to increases in greenhouse gases and decreases in stratospheric ozone, with ozone losses dominating in the lower stratosphere, and more-or-less equal contributions in the upper stratosphere (for the period 1979–1999) [*Shine et al.*, 2003]. The recent flattening of trends throughout the stratosphere over the last decade seen in Figures 1 and 7 (with near constant temperatures after 1995) is most interesting, given the continued increases in CO_2, combined with relatively small changes in stratospheric ozone over this period [*World Meteorological Organization*, 2006].

The analyses here have not included detailed discussions of the QBO variations in stratospheric temperatures, which have magnitudes up to ±4 K and span the tropics to middle latitudes [e.g., *Crooks and Gray*, 2005]. The QBO is relatively easy to isolate statistically, as there are over 10 complete cycles in the satellite observational record. We have also not discussed the 11-year solar cycle variations in stratospheric temperature, which have been recently discussed in the work of *Randel et al.* [2009a]; both the radiosonde and satellite data sets show coherent solar variations throughout the stratosphere in low latitudes (~30°N–30°S), with amplitudes ranging from 0.5 K in the lower stratosphere to 1.0 K in the upper stratosphere. The ENSO effects on zonal mean temperature in the lower stratosphere (Figure 2b) are also an important component of interannual variability in this region (Figure 3). We note that similar behavior is observed in stratospheric ozone observations and that such temperature and ozone variations are found in a recent chemistry-climate model simulation that incorporates observed sea surface temperature forcing [*Randel et al.*, 2009b]. *Marsh and Garcia* [2007] suggest that there can be confusion of the ENSO and solar signal components in short data records, and neglecting this effect may result in overestimating the ozone solar signal in the tropical lower stratosphere.

Global satellite measurements of stratospheric water vapor are available for 1993–2010, and these data allow accurate mapping of the seasonal cycle and interannual variability over this period. Interannual changes in water vapor show strong coherence throughout the stratosphere, with anomalies originating near the tropical tropopause and propagating latitudinally in the lower stratosphere and vertically in the tropics (advected by the Brewer-Dobson circulation). The observed water vapor anomalies are highly correlated with temperatures near the equatorial cold point tropopause, and the observations for 1993–2010 are consistent with simple dehydration of air entering the stratosphere across the cold point (as simulated in Lagrangian trajectory calculations of *Fueglistaler and Haynes* [2005]). There was an observed drop in stratospheric water vapor (~0.4 ppmv) and cold point temperature (~1 K) after 2001, which has continued to the present, albeit modulated by the QBO with a suggestion of

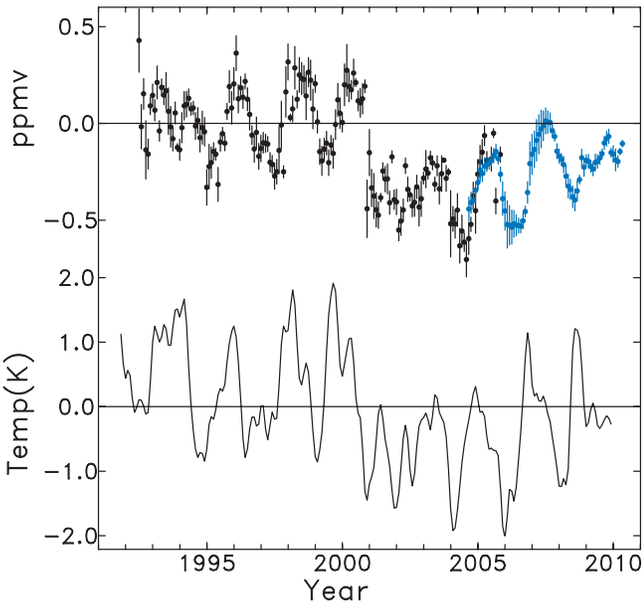

Plate 6. (top) Time series of lower stratosphere (82 hPa) water vapor anomalies from HALOE + MLS data, as in Plate 5a. (bottom) Time series of tropical cold-point tropopause temperature anomalies, derived from several radiosonde stations, as described in the text. The correlation coefficient is 0.75, with water vapor lagging the temperatures by 2 months.

recent increasing values. The cooling associated with the change after 2001 is largest in a narrow vertical layer centered near the cold point and may be associated with a corresponding increase in tropical upwelling [*Randel et al.*, 2006]. However, given the short observational record, it is difficult to link this step-like change to any decadal-scale trends in water vapor, tropopause temperature, or upwelling.

As noted above, the longest record of stratospheric water vapor comes from the balloon measurements at Boulder, Colorado, beginning in 1980 (as recently reviewed in the work of *Scherer et al.* [2008]). These data show positive trends over the period 1980–2006, which seems at odds with the near-zero or cooling trends near the tropical tropopause over this period (Plate 1) [see also *Seidel et al.*, 2001]. Interpretation of the Boulder record is also hampered by disagreement with trends derived from the HALOE record for the overlap period 1992–2005 [*Scherer et al.*, 2008]. *Fueglistaler and Haynes* [2005] also show that the Boulder trends for 1980–2004 are difficult to reconcile with Lagrangian trajectory results. Thus, while the 1993–2010 satellite record suggests a relatively simple interpretation of stratospheric water vapor changes linked to equatorial tropopause temperatures, interpretation of the longer record of Boulder balloon measurements remains a topic of ongoing research.

APPENDIX A: LINEAR REGRESSION ANALYSIS

Statistical climate signals in the temperature data are derived using a multivariate linear regression analysis, as in the work of *Ramaswamy et al.* [2001]. The statistical model includes terms to account for linear trends, solar cycle (using the solar F10.7 radio flux as a proxy), ENSO (using the Multivariate ENSO Index from the NOAA Climate Diagnostics Center, http://www.cdc.noaa.gov/people/klaus.wolter/MEI/, with atmospheric temperatures lagged by 1 month), plus two orthogonal time series to model the QBO [*Wallace et al.*, 1993]. We omit 2 years after each of the large volcanic eruptions (El Chichon in April 1982 and Mount Pinatubo in June 1991) from the regression analysis, to avoid influence from the associated large transient warming events. Uncertainty estimates for the statistical fits are calculated using a bootstrap resampling technique [*Efron and Tibshirani*, 1993], which includes the effects of serial autocorrelation.

Acknowledgments. We thank Rolando Garcia and Eric Jensen for comments that helped improve the manuscript and appreciate a constructive review provided by Dian Seidel. Fei Wu provided assistance with data analysis and graphics. This work was partially supported by the NASA ACMAP Program. The National Center for Atmospheric Research is operated by the University Corporation for Atmospheric Research, under sponsorship of the National Science Foundation.

REFERENCES

Austin, J., et al. (2009), Coupled chemistry climate model simulations of stratospheric temperatures and their trends for the recent past, *Geophys. Res. Lett.*, *36*, L13809, doi:10.1029/2009GL038462.

Brewer, A. W. (1949), Evidence for a world circulation provided by measurements of helium and water vapor distribution in the stratosphere, *Q. J. R. Meteorol. Soc.*, *75*, 351–363.

Calvo Fernandez, N., et al. (2004), Analysis of the ENSO signal in tropospheric and stratospheric temperatures observed by MSU, 1979–2000, *J. Clim.*, *17*, 3934–3946.

Christy, J. R., R. W. Spencer, W. B. Norris, W. D. Braswell, and D. E. Parker (2003), Error estimates of version 5.0 of MSU-AMSU bulk atmospheric temperatures, *J. Atmos. Oceanic Technol.*, *20*, 613–629.

Crooks, S. A., and L. J. Gray (2005), Characterization of the 11-year solar signal using a multiple regression analysis of the ERA-40 dataset, *J. Clim.*, *18*, 996–1015.

Dvortsov, V. L., and S. Solomon (2001), Response of the stratospheric temperatures and ozone to past and future increases in stratospheric humidity, *J. Geophys. Res.*, *106*, 7505–7514.

Efron, B., and R. J. Tibshirani (1993), *An Introduction to the Bootstrap*, 436 pp., Chapman and Hall, London.

Eyring, V., et al. (2006), Assessment of temperature, trace species, and ozone in chemistry-climate model simulations of the recent past, *J. Geophys. Res.*, *111*, D22308, doi:10.1029/2006JD007327.

Forster, P. M. d. F., and K. P. Shine (1999), Stratospheric water vapour changes as a possible contributor to observed stratospheric cooling, *Geophys. Res. Lett.*, *26*, 3309–3312.

Free, M., and J. K. Angell (2002), Effect of volcanoes on the vertical temperature profile in radiosonde data, *J. Geophys. Res.*, *107* (D10), 4101, doi:10.1029/2001JD001128.

Free, M., and D. J. Seidel (2009), Observed El Niño–Southern Oscillation temperature signal in the stratosphere, *J. Geophys. Res.*, *114*, D23108, doi:10.1029/2009JD012420.

Free, M., D. J. Seidel, J. K. Angell, J. Lanzante, I. Durre, and T. C. Peterson (2005), Radiosonde Atmospheric Temperature Products for Assessing Climate (RATPAC): A new data set of large-area anomaly time series, *J. Geophys. Res.*, *110*, D22101, doi:10.1029/2005JD006169.

Fueglistaler, S., and P. H. Haynes (2005), Control of interannual and longer-term variability of stratospheric water vapor, *J. Geophys. Res.*, *110*, D24108, doi:10.1029/2005JD006019.

Fueglistaler, S., M. Bonazzola, P. H. Haynes, and T. Peter (2005), Stratospheric water vapor predicted from the Lagrangian temperature history of air entering the stratosphere in the tropics, *J. Geophys. Res.*, *110*, D08107, doi:10.1029/2004JD005516.

Gaffen, D. J. (1994), Temporal inhomogeneities in radiosonde temperature records, *J. Geophys. Res.*, *99*, 3667–3676.

Garcia, R. R., D. R. Marsh, D. E. Kinnison, B. A. Boville, and F. Sassi (2007), Simulations of secular trends in the middle atmosphere, 1950–2003, *J. Geophys. Res.*, *112*, D09301, doi:10.1029/2006JD007485.

Haimberger, L., C. Tavolato, and S. Sperka (2008), Towards elimination of the warm bias in historic radiosonde temperature records—Some new results from a comprehensive intercomparison of upper air data, *J. Clim.*, *21*, 4587–4606.

Intergovernmental Panel on Climate Change (2007), Climate Change 2007: The Physical Science Basis. Contribution of Working Group I to the Fourth Assessment Report of the Intergovernmental Panel on Climate Change, edited by S. Solomon, et al., 996 pp., Cambridge Univ. Press, New York.

Keckhut, P., et al. (2004), Review of ozone and temperature lidar validations performed within the framework of the Network for the Detection of Stratospheric Change, *J. Environ. Monit.*, *6*, 721–733.

Labitzke, K. G., and H. van Loon (1999), *The Stratosphere: Phenomena, History and Relevance*, 179 pp., Springer, New York.

Lanzante, J., S. Klein, and D. J. Seidel (2003a), Temporal homogenization of monthly radiosonde temperature data. Part I: Methodology, *J. Clim.*, *16*, 224–240.

Lanzante, J., S. Klein, and D. J. Seidel (2003b), Temporal homogenization of monthly radiosonde temperature data. Part II: Trends, sensitivities and MSU comparisons, *J. Clim.*, *16*, 241–262.

Lanzante, J. R. (2009), Comment on "Trends in the temperature and water vapor content of the tropical lower stratosphere: Sea surface connection" by Karen H. Rosenlof and George C. Reid, *J. Geophys. Res.*, *114*, D12104, doi:10.1029/2008JD010542.

Marsh, D. R., and R. R. Garcia (2007), Attribution of decadal variability in lower-stratospheric tropical ozone, *Geophys. Res. Lett.*, *34*, L21807, doi:10.1029/2007GL030935.

Mears, C. A., and F. J. Wentz (2009), Construction of the Remote Sensing Systems V3.2 atmospheric temperature records from the MSU and AMSU microwave sounders, *J. Atmos. Oceanic Technol.*, *26*, 1040–1056.

Mote, P. W., K. H. Rosenlof, M. E. McIntyre, E. S. Carr, J. C. Gille, J. R. Holton, J. S. Kinnersley, H. C. Pumphrey, J. M. Russell III, and J. W. Waters (1996), An atmospheric tape recorder: The imprint of tropical tropopause temperatures on stratospheric water vapor, *J. Geophys. Res.*, *101*, 3989–4006.

Nash, J. (1988), Extension of explicit radiance observations by the Stratospheric Sounding Unit into the lower stratosphere and lower mesosphere, *Q. J. R. Meteorol. Soc.*, *114*, 1153–1171.

Nash, J., and G. F. Forrester (1986), Long-term monitoring of stratospheric temperature trends using radiance measurements obtained by the TIROS-N series of NOAA spacecraft, *Adv. Space Res.*, *6*, 37–44.

Oltmans, S. J., and D. J. Hofmann (1995), Increase in lower-stratospheric water vapour at a mid-latitude Northern Hemisphere site from 1981 to 1994, *Nature*, *374*, 146–149.

Oltmans, S. J., H. Vömel, D. J. Hofmann, K. H. Rosenlof, and D. Kley (2000), The increase in stratospheric water vapor from balloonborne, frostpoint hygrometer measurements at Washington, D.C., and Boulder, Colorado, *Geophys. Res. Lett.*, *27*(21), 3453–3456.

Oman, L., D. W. Waugh, S. Pawson, R. S. Stolarski, and J. E. Nielsen (2008), Understanding the changes of stratospheric water vapor in coupled chemistry-climate model simulations, *J. Atmos. Sci.*, *65*, 3278–3291.

Ramaswamy, V., et al. (2001), Stratospheric temperature trends: Observations and model simulations, *Rev. Geophys.*, *39, 71–122.*

Ramaswamy, V., M. Schwarzkopf, W. J. Randel, B. D. Santer, B. J. Soden, and G. L. Stenchikov (2006), Anthropogenic and natural influences in the evolution of lower stratospheric cooling, *Science*, *311*, 1138–1141.

Randel, W. J., and F. Wu (1999), Cooling of the Arctic and Antarctic polar stratospheres due to ozone depletion, *J. Clim.*, *12*, 1467–1479.

Randel, W. J., and F. Wu (2006), Biases in stratospheric and tropospheric temperature trends derived from historical radiosonde data, *J. Clim.*, *19*, 2094–2104.

Randel, W. J., F. Wu, S. Oltmans, K. Rosenlof, and G. Nedoluha (2004), Interannual changes of stratospheric water vapor and correlations with tropical tropopause temperatures, *J. Atmos. Sci.*, *61*, 2133–2148.

Randel, W. J., F. Wu, H. Vömel, G. Nedoluha, and P. Forster (2006), Decreases in stratospheric water vapor since 2001: Links to changes in the tropical tropopause and the Brewer-Dobson circulation, *J. Geophys. Res.*, *111*, D12312, doi:10.1029/2005JD006744.

Randel, W. J., et al. (2009a), An update of observed stratospheric temperature trends, *J. Geophys. Res.*, *114*, D02107, doi:10.1029/2008JD010421.

Randel, W. J., R. R. Garcia, N. Calvo, and D. Marsh (2009b), ENSO influence on zonal mean temperature and ozone in the tropical lower stratosphere, *Geophys. Res. Lett.*, *36*, L15822, doi:10.1029/2009GL039343.

Read, W. G., et al. (2007), Aura Microwave Limb Sounder upper tropospheric and lower stratospheric H_2O and relative humidity with respect to ice validation, *J. Geophys. Res.*, *112*, D24S35, doi:10.1029/2007JD008752.

Reid, G. C. (1994), Seasonal and interannual temperature variations in the tropical stratosphere, *J. Geophys. Res.*, *99*, 18,923–18,932.

Rosenlof, K. H., and G. C. Reid (2008), Trends in the temperature and water vapor content of the tropical lower stratosphere: Sea surface connection, *J. Geophys. Res.*, *113*, D06107, doi:10.1029/2007JD009109.

Russell, J. M., III, L. L. Gordley III, J. H. Park, S. R. Drayson, W. D. Hesketh, R. J. Cicerone, A. F. Tuck, J. E. Frederick, J. E. Harries, and P. J. Crutzen (1993), The Halogen Occultation Experiment, *J. Geophys. Res.*, *98*, 10,777–10,797.

Scherer, M., H. Vömel, S. Fueglistaler, S. J. Oltmans, and J. Staehelin (2008), Trends and variability of midlatitude stratospheric water vapour deduced from the re-evaluated Boulder balloon series and HALOE, *Atmos. Chem. Phys.*, *8*, 1391–1402.

Seidel, D. J., and J. R. Lanzante (2004), An assessment of three alternatives to linear trends for characterizing global atmospheric temperature changes, *J. Geophys. Res.*, *109*, D14108, doi:10.1029/2003JD004414.

Seidel, D. J., R. J. Ross, J. K. Angell, and G. C. Reid (2001), Climatological characteristics of the tropical tropopause as revealed by radiosondes, *J. Geophys. Res.*, *106* (D8), 7857–7878.

Shine, K. P., et al. (2003), A comparison of model-simulated trends in stratospheric temperatures, *Q. J. R. Meteorol. Soc.*, *129*, 1565–1588.

Shine, K. P., J. J. Barnett, and W. J. Randel (2008), Temperature trends derived from Stratospheric Sounding Unit radiances: The effect of increasing CO_2 on the weighting function, *Geophys. Res. Lett.*, *35*, L02710, doi:10.1029/2007GL032218.

Soden, B. J., R. T. Wetherald, G. L. Stenchikov, and A. Robock (2002), Global cooling after the eruption of Mount Pinatubo: A test of climate feedback by water vapor, *Science*, *296*, 727–730, doi:10.1126/science.296.5568.727.

Solomon, S., et al. (2010), Contributions of stratospheric water vapor to decadal changes in the rate of global warming, *Science*, *327*, 1219–1223, doi:10.1126/science.1182488.

SPARC CCMVal (2010), SPARC report on the evaluation of chemistry-climate models, edited by V. Eyring, T. G. Shepherd, and D. W. Waugh, *WMO/TD-No. 1526*, World Meteorol. Organ., Geneva, Switzerland. (Available at http://www.atmosp.physics.utoronto.ca/SPARC)

Stratospheric Processes and Their Role in Climate (SPARC) (2000), SPARC Assessment of Upper Tropospheric and Stratospheric Water Vapor, edited by D. Kley, J. M. Russell III, and C. Phillips, *SPARC Rep. 2*, 312 pp., World Meteorol. Organ., Geneva, Switzerland.

Wallace, J. M., R. L. Panetta, and J. Estberg (1993), Representation of the equatorial quasi-biennial oscillation in EOF phase space, *J. Atmos. Sci.*, *50*, 1751–1762.

World Meteorological Organization (2006), Scientific assessment of ozone depletion: 2006, *Rep. 47*, Global Ozone Res. and Monit. Proj., Geneva, Switzerland.

Yoden, S., M. Taguchi, and Y. Naito (2002), Numerical studies on time variations of the troposphere-stratosphere coupled system, *J. Meteorol. Soc. Jpn.*, *80*, 811–830.

Yulaeva, E., and J. M. Wallace (1994), The signature of ENSO in global temperature and precipitation fields derived from the microwave sounding unit, *J. Clim.*, *7*, 1719–1736.

W. J. Randel, Atmospheric Chemistry Division, National Center for Atmospheric Research, PO Box 3000 Boulder, CO 80307-3000, Boulder, CO 80307, USA. (randel@ucar.edu)